Biointerface Research in Applied Chemistry
Open-Access Journal (ISSN: 2069-5837)

Article
Volume 13, Issue 3, 2023, 212
https://doi.org/10.33263/BRIAC133.212

Design and *In Vitro* Optimization of the Gastroretentive Microparticles Using Ethylcellulose and Eudragit

Meenakshi Bhatia [1], Rameshwar Dass [2,*], Goutam Rath [3]

[1] Department of Pharmaceutics, Guru Jambheshwar University of Science and Technology, Hisar, Haryana, India; meenaxibhatia@gmail.com (M.B.);
[2] Guru Gobind Singh College of Pharmacy, Yamunanagar, Haryana, India; rdladwa01@gmail.com (R.D.);
[3] Department of Pharmaceutics, Siksha O Anusandhan (Deemed to be University), Bhubaneswar, Odisha, India; goutamrath123@gmail.com (G.R.);
* Correspondence: rdladwa01@gmail.com (R.D.);

Scopus Author ID 7005235468
Received: 31.03.2022; Accepted: 11.05.2022; Published: 5.06.2022

Abstract: The biocompatible and bioadhesive polymers ethylcellulose and eudragit S100 are often used for controlled delivery of drugs in low pH conditions. Recent research focuses on designing and optimizing multiparticulate floating and bioadhesive systems using a central composite approach. Gastro-retentive floating microparticles of ethylcellulose and eudragit S100 containing itopride hydrochloride (ITH) were prepared using a solvent evaporation method. The impact of several process variables, including drug-polymer ratio, were studied on physicochemical parameters such as drug entrapment efficiency, particle size, bioadhesion, and release by employing a central composite design strategy. The experimental results were in good agreement with the predicted values of the optimization technique. The optimized microparticles had a 94.77 % drug entrapment efficiency, a particle size of 259.2 µm, 96.98 % drug release in simulated stomach fluid (pH 1.2) after 12 hours, and an 8-hour floating lag time. An accelerated stability analysis was conducted on the optimized formulation according to ICH criteria, and no significant changes in drug quantity were identified during storage. The microparticulate formulation containing ethylcellulose to eudragit S100 (in the ratio of 9:3) prepared by solvent evaporation technique displayed suitable pharmaceutical characteristics for controlled gastro retentive delivery of ITH. Furthermore, the results of the stability studies indicated that the developed formulation had not undergone any major changes under stress.

Keywords: gastro-retentive; prokinetic; microparticle; eudragit; ethylcellulose.

1. Introduction

Oral delivery remains the most preferred route for drug administration because of its convenience, cost-effectiveness, and patient compliance [1, 2]. In recent years significant advancements have been made in oral drug delivery to facilitate site-specific controlled drug delivery [3-6]. Gastro retentive drug delivery systems (GRDDS) offer a unique opportunity for formulation scientists for the localized action in the stomach [7, 8]. Over the years, numbers of GRDDS delivery dosage forms, including high-density systems [9], floating systems [10], bioadhesive systems [11, 12], and expandable systems [13], have been explored for the site-specific drug release over a defined period. Single-unit and multiple-unit systems have been documented in the literature [14]. Multi-unit formulations provide several advantages over single-unit floating dosage forms, including preventing drug concentration changes at static

and dynamic states, avoiding performance loss owing to particle impact, and providing predictable release kinetics of encapsulated bioactive [15-17].

The choice of drug candidate and polymer is critical to the therapeutic outcome of GRDDS. Itopride hydrochloride (ITH) is a highly selective acetylcholine esterase inhibitor and dopamine D2 receptor antagonist that operates in the upper GI tract (Figure 1). It can speed up the emptying of the stomach [18-20]. Oral bioavailability, on the other hand, is roughly 60% due to substantial pre-systemic metabolism [21]. These characteristics support the development of a gastro-retentive formulation of ITH for improved therapeutic efficacy. Ethylcellulose (EC) and eudragit S100 (ES), because of their stated biodegradability and biocompatibility, were chosen as polymer components in this investigation. Furthermore, the pH-dependent drug release of EC and ES has been thoroughly explored [22, 23]. In the current investigation, a novel particulate gastro-retentive formulation based on a combination of floating/bioadhesive mechanisms was developed and characterized. Finally, in central composite design, a collection of statistical/mathematical models is used to design experiments and determine the best-fit model for independent variables of floating microparticles for improved outcomes [24, 25].

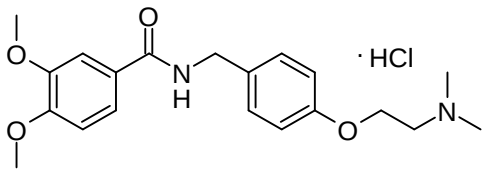

Figure 1. Chemical structure of ITH.

2. Materials and Methods

ITH and ES were received as a gift sample from Abbott Labs, Himachal Pradesh. EC and polyvinyl acrylate were purchased from SD Fine Chem Limited, Mumbai. The rest of the chemical substances were of analytical grade.

2.1. Microparticles preparation.

The desired amounts of ITH in the polymer solution (EC and ES) were dissolved in a minimal volume of ethanol and dichloromethane (1:1), as shown in Table 1. This solution was added to 70 ml of 0.57 % w/v PVA solution in distilled water using a 24-gauge 10ml hypodermic syringe. To consolidate and evaporate the solvent mixture, the emulsion was agitated at 500 rpm for 2 hours with a mechanical stirrer. The resultant suspension was collected, washed with distilled water, and air-dried overnight at 25-30 °C in a vacuum desiccator with calcium chloride to dry discrete microparticles [26, 27].

Table 1. Formulation design for preliminary studies.

Formulation	Drug (mg)	EC (mg)	ES (mg)	Appearance	% Yield	Particle size (µm)	Entrapment efficiency (%)
M1	50	500	100	Spherical	75	430	70.87±0.22
M2	50	500	150	Spherical	78	510	78.31±0.32
M3	50	500	250	Irregular shaped	79	635	73.44±0.21
M4	50	250	100	Mixed	76	325	76.30±0.32
M5	50	250	150	Irregular shaped	78	345	70.57±0.25
M6	50	250	250	Foam	77	380	73.44±0.35

2.2. Experimental design.

The response surface method was used to explore the effect of a large number of independent/dependent factors. Table 2 shows the formulation variable with levels determined based on the early investigations' findings. In the creation of microparticles, two independent parameters were considered: EC (A) and ES (B), while active substance entrapment efficiency, % drug release after 12 hours, and particle size were dependent responses [28, 29].

Table 2. Process parameter levels were used in the formulation design.

Code	Parameter	Levels		
		-1	**0**	**1**
A	EC	250	50	375
B	ES	100	250	175

Table 3. Central composite design with detected response.

Formulation code	Run	EC (mg)	ES (mg)	% Entrapment	% Release	Avg. particle size (microns)
M1	1	250.00	100.00	75.33	96.59	215.0
M2	4	500.00	100.00	84.4	92.51	262.9
M3	2	250.00	250.00	70.63	94.72	233.2
M4	5	500.00	250.00	94.77	96.98	259.2
M5	6	198.22	175.00	66.31	96.62	209.7
M6	8	551.78	175.00	89.03	94.39	248.1
M7	3	375.00	68.93	72.16	93.62	238.9
M8	9	375.00	281.07	86.46	97.33	245.3
M9	7	375.00	175.00	73.31	96.37	233.7

The examined responses of drug entrapment (%), particle size (µm), and % drug release after 12 hours are in Table 3. The effects of independent factors on modeled responses using the polynomial equation involving independent and interaction factors for measured responses studied in this study based on lack of fit, model analysis, and R^2 evaluations. The quadratic model was constructed through a central composite design to model the impacts of independent variables on active agent entrapment (percent), % drug release over 12 hours, and particle size (µ):

$$Y = b_0 + b_1A + b_2B + b_3AB + b_4A^2 + b_5B^2$$

The regression coefficients (b_1, b_2, b_3, b_4, and b_5) are in response to Y, with the intercept (b0). Individual effects were A and B, quadratic effects were A^2 and B^2, and the interaction effect was AB. To determine the model's significance ($p<0.05$), a one-way ANOVA was used. The F-test was used to examine individual response parameters. The outcome of independent variant (here EC and ES) on the measured responses (here drug entrapment, particle size, and % release afterward 12 hours) was investigated using contour plots and surface dependent plots.

2.3. Percentage yield.

The quantity of microparticles obtained from each formulation and the initial ingredients (starting weight) can be used to compute the % of production yield [30], as shown in the following equation:

$$\text{Yield (\%)} = \frac{\text{Wt. of microparticles}}{\text{Total wt. of drug and polymer}} \times 100$$

2.4. Surface morphology analysis.

The scanning electron microscope was used to examine the microparticles' surface morphologies using (Jeol, JSM-6100, Japan) [19] Figure 2.

2.5. Particle size analysis.

The size of produced microparticles was assessed in triplicates using the microscopy method. Microparticles were shaken with solvent to prepare a slide and observed under the calibrated eyepiece on microscope size [31]. The particle size distribution was determined by the plotting frequency of particles versus particles. The mean particle size was estimated, as shown in Figure 3.

2.6. Drug content.

Drug content was measured in triplicates using a previously published method [32, 33]. An accurately weighed amount of 25 mg microparticles was crushed in acrylic mortar-pestle. The powdered microparticles were immersed in 10 ml of 0.1 N HCl with continual sonication for 2 hours at 37 ± 0.5 C. The drug content in the filtrate was tested using a UV-spectroscopy at 258 nm after sonication. The drug entrapment (DE, %) was determined using the following formula:

$$\text{DE (\%)} = \frac{\text{Actual drug content}}{\text{Theoretical drug content}} \times 100$$

2.7. UV- calibration curve.

The calibration curve of ITH was prepared in 0.1N hydrochloric acid solution with the stock solution of 100 mcg/ml in HCl. Aliquots of stock solution were converted into different dilution rages from 10-60 mcg/ml. The lambda max was verified using a 10ppm solution and scanned between 400-200 nm. The absorbance of the above solutions was taken against the blank (without adding the drug). A graph was plotted between absorbance and concentration [34].

2.8. In-vitro buoyancy study.

The floating behavior of microparticles was investigated in triplicate using a method that has previously been published [35]. At 37±0.5 ˚C, 50 microparticles were put in 150 ml of 0.1 N HCl. During 12 hours, the number of microparticles floating and the floating duration were determined at a constant time period.

2.9. In-vitro drug release studies.

A dissolution device, USP dissolution apparatus-1 [36], was used to examine the drug's in-vitro release from produced microparticles. An amount of microparticles equal to 50 mg of the drug was added to 900 ml of 0.1N HCl (pH 1.2) and stirred at 100 rpm at 37±0.5 ˚C. Throughout the experiment, a 5 mL sample was collected at regular intervals, and the equivalent amount of new dissolution medium was replaced in the dissolution tank to maintain the sink condition. The obtained aliquots were filtered and diluted appropriately for UV-spectroscopic analysis at 258 nm.

2.10. Kinetics and mechanism of in-vitro drug release.

In-vitro drug release data from several microparticle formulations containing ITH were analyzed using kinetic models such as zero order, first order, Higuchi, and Korsmeyer–Peppas [37, 38]. F = K0t in the zero-order model. ln (1F) = K1t, is the first-order model. F = KHt1/2 is the Higuchi model, Korsmeyer–Peppas model: F = KPtn; n is the release exponent, indicative of the drug release mechanism, where F fraction of medication released in time t and K (rate constant). The Korsmeyer–Peppas model was used to distinguish between conflicting release mechanisms in these formulations' in-vitro drug release behavior. The Fickian release is indicated by a value of n 0.43 for spheres. The non-Fickian release is indicated by an n value between 0.43 and 0.85. (both diffusions controlled and swelling controlled drug release). It's case-II transport when n 0.85, and it involves polymer breakdown and polymeric chain expansion or relaxation.

2.11. Fourier transform infrared spectroscopy.

As KBr pellets, samples were reduced to powder using Fourier transform infrared spectroscopes [39] (Perkin Elmer Spectrum, BX II). Pellets were placed in sample holders, and spectral scanning was obtained in the wavelength range between 4000 and 400 cm*1.

2.12. Stability studies of the optimized formulation.

According to the International Conference on Harmonization (ICH) rules, the improved formulation was retained for 3 months for an accelerated stability assessment [40]. Microparticles were wrapped in a laminated aluminum foil and preserved in a stability chamber at a temperature of 40±2 ˚C and relative humidity of 75+5 %. After 0, 30, 60, and 90 days, samples were extracted, and a paired Student's t-test was used to look for any statistical differences in adhesion retention periods, floating properties, and drug content. At $p<0.05$, differences were judged significant [41].

3. Results and Discussion

3.1. Preliminary studies.

Table 1 shows the formulation design for preliminary studies. When the liquid temperature was elevated above 35 °C, no microparticles were formed (M6). Solid spumes but no microparticles were formed. The formation of microparticles was also found to be affected by the stirring speed. Increased stirring speed to 500 rpm (M5) produced approximately spherical microparticles; however, when speed was increased to 1000 rpm (M4), microparticles created during cross-linking collided with great energy and were destroyed.

3.2. Optimization.

The design expert's software offered a total of 9 experimental trial formulations for two components, EC (A) and ES (B), which were modified at three distinct levels for the central composite design. For the optimization response parameters in this investigation, the impacts of independent factors on drug entrapment (%), particle size (µm), and released after 12 hours (%) were studied. Table 3 shows a summary of the experimental plan as well as observed results.

Table 4. ANOVA for Response Surface Quadratic Model (drug entrapment).

Source	Sum of Squares	df	Mean Square	F Value	p-value
Model	715.39	5	143.08	10.17	0.0424
A-A EC	533.68	1	533.68	37.92	0.0086
B-B ES	83.81	1	83.81	5.96	0.0925
AB	56.78	1	56.78	4.03	0.1382
A^2	24.10	1	24.10	1.71	0.2819
B^2	39.79	1	39.79	2.83	0.1913
Residual	42.22	3	14.07		
Cor Total	757.61	8			

The model proposes the following polynomial equation for % drug entrapment:

$$R1 = 73.31+8.17*A+3.24*B+3.77*A*B+2.88*A^2+3.70*B^2$$

The model's F-value of 10.17 indicates that it is statistically significant (p 0.0424) (Table 4). A and B are important model terms in this scenario. The 0.9443 'Pred R Squared' is in reasonable agreement with the 0.8514 Adj R-squared. The signal-to-noise ratio is measured by 'Adeq Precision,' and a ratio of 8.992 indicates a good signal.

Table 5. ANOVA for Response Surface Quadratic Model (% release).

Source	Sum of Squares	df	Mean Square	F Value	p-value
Model	21.77	5	4.35	10.32	0.0416
A-A EC	3.09	1	3.09	7.33	0.0734
B-B ES	7.70	1	7.70	18.24	0.0236
AB	10.05	1	10.05	23.81	0.0165
A^2	0.74	1	0.74	1.76	0.2768
B^2	0.79	1	0.79	1.86	0.2656
Residual	1.27	3	0.42		
Cor Total	23.04	8			

The following polynomial equation for % release is proposed by the model:

$$R2 = 96.37-0.62*A+0.98*B+1.59*A*B-0.50*A^2-0.52*B^2$$

The model F-value of 10.32 suggests the model is significant ($p < 0.0416$) (Table 5). In this case, A, B, and AB are significant model terms. The 'Pred R -Squared' of 0.9450 is in reasonable agreement with the Adj R-squared of 0.8534. The ratio of 8.992 indicates an adequate signal.

Table 6. ANOVA for Response Surface Quadratic Model (particle size).

Source	Sum of Squares	df	Mean Square	F Value	p-value
Model	2443.39	5	488.68	9.66	0.0455
A-A EC	2054.59	1	2054.59	40.60	0.0078
B-B ES	69.33	1	69.33	1.37	0.3263
AB	119.90	1	119.90	2.37	0.2214
A^2	1.16	1	1.16	0.023	0.8893
B^2	103.64	1	103.64	2.05	0.2478
Residual	151.81	3	50.60		
Cor Total	2595.20	8			

The polynomial equation for particle size proposed by the model is as follows:

$$R3 = 233.70+16.03*A+2.94*B-5.48*A*B-0.63*A2+5.97*B2$$

The F-value of 9.66 for the model indicates that it is significant ($p < 0.0455$) (Table 6). Significant model terms in this situation are A, B, and AB. The 'Pred R-Squared' of 0.9415 is in good agreement with the Adj R-squared of 0.8440. The ratio of 8.233 suggests a good signal.

Table 7. All response variables in terms of the actual and predicted value.

Standard Order	R3 Particle size		R2 % Release		R1 % Entrapment	
	Actual Value	Predicted Value	Actual Value	Predicted Value	Actual Value	Predicted Value
M1	215.00	214.59	96.59	96.57	75.33	72.25
M2	262.90	257.59	92.51	92.16	84.40	81.05
M3	233.20	231.43	94.72	95.36	70.63	71.19
M4	259.20	252.53	96.98	97.29	94.77	95.06
M5	209.70	209.77	96.62	96.24	66.31	67.52
M6	248.10	255.10	94.39	94.48	89.03	90.62
M7	238.90	241.47	93.62	93.94	72.16	76.13
M8	245.30	249.80	97.33	96.72	86.46	85.28
M9	233.70	233.70	96.37	96.37	73.31	73.31

The results of investigated responses (drug entrapment, particle size, and percent release after 12 hours) were found to be within limits for all of these formulations proposed by the central composite design. Table 7 shows the actual and predicted responses for all response variables studied in this study and the parentage of prognosis errors. Linear correlation plots between the residuals versus predicted values are present in Figures 2a, 2c, and 2e, and their corresponding residual plots showing the scatter of the actual, the predicted response variables are presented in Figures 2b, 2d, and 2f.

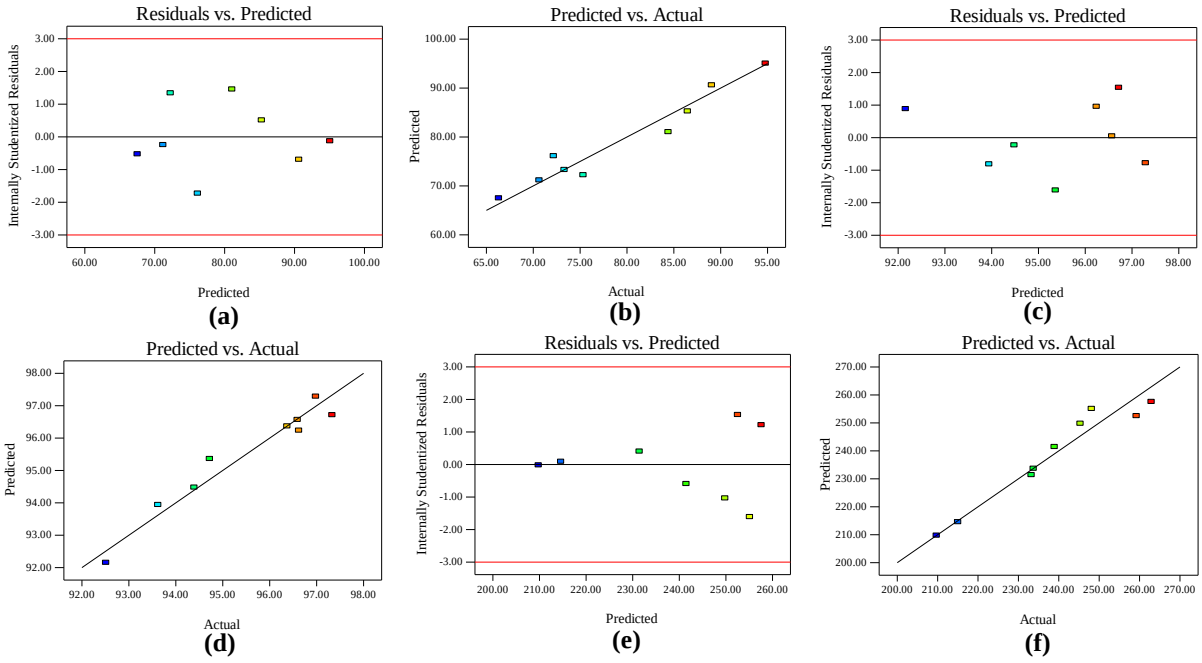

Figure 2. (**a**) Entrapment, (**c**) particle size, and (**e**) release linear correlation plots for the residuals versus predicted values; (**b**) entrapment, (**d**) particle size, and (**f**) release residual plots for the scatter of the actual, the predicted response variables.

The three-dimensional response surface graph is particularly useful for learning about the main and interaction effects of the independent components. The three-dimensional response surface graph, Figures 3a and 3c, connected to drug entrapment efficiency, shows that as the EC ratio (A) and ES (B) ratios grow, so does drug entrapment efficiency. Particle size

increases as both polymer ratios increase, according to the three-dimensional response surface graph, Figures 3c and 3d (A and B). The three-dimensional response surface graph of percent release after 12 hours and the drug to polymer ratio, on the other hand, reveals a decline in percent drug release after 12 hours.

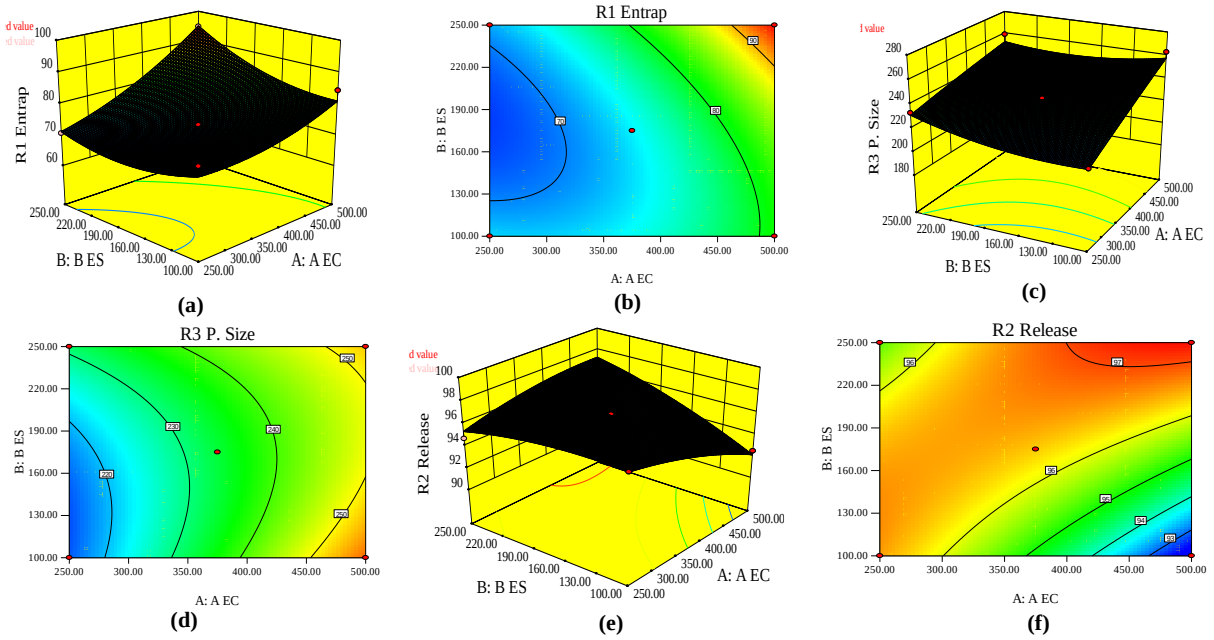

Figure 3. 3D surface response plots for drug entrapment efficiency (**a** and **b**), particle size (**c** and **d**), and release rate (**e** and **f**).

The ideal values of the parameters for maximum entrapment, percentage release, and least particle size were determined using the software's estimation profiler. Finally, the best EC (A = 500), ES (B = 250), and constant stirring speed (500 rpm) were found from pre-trials. These figures indicate 95.06 % drug entrapment, 252.53 microns particle size, and 97.29 % release. These expected response values were confirmed in vitro with ITH-loaded microparticles made using previously optimized process parameters, yielding an average of 94.77 % drug entrapment, 259.2 microns size, and 96.98 % release. The projected drug entrapment, particle size, and release model have 99.69 %, 102.64 %, and 99.68 % validity, respectively.

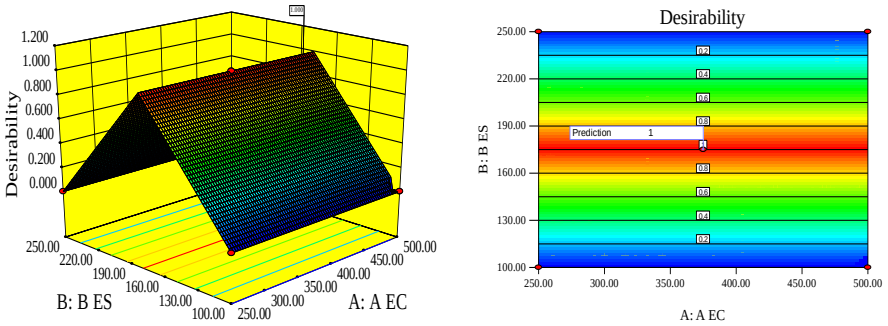

Figure 4. Desirability 3D and contour graph of the particle system.

The desirability ramp for optimization of particles is shown in Figure 4; when the target of ES was set at 175, then the values of EC gave 26 solutions. While increasing EC concentration, the entrapment, particle size, and release were between 66-94%, 92-97.33%,

and 209-262 microns. The predicted value for solution1 was entrapment (73.31), particle size (233.7), and 96.37%, respectively, as shown in Figure 4.

3.3. Drug entrapment efficiency.

Depending on the formulation composition, the drug entrapment efficiency of formed ITH-loaded microparticles ranged from 66.31 to 94.77 (Tables 3 and 7). An increased proportion of ITH-EC and ES100 ratio was shown to promote drug entrapment in microparticles, but an increase in rpm decreased drug entrapment.

3.4. Particle size.

The size of dried ITH entrapped EC, and ES100 microparticles were assessed using a microscopic technique for each formulation. The mean particle size distribution ranged from 209.70 to 262.90 microns (Table 5). Adding more drug-polymer ratios to formulations was found to increase particle size. As the stirring rpm was increased, the particle subdivision caused by the generation of more energy decreased.

3.5. Bioadhesion study.

The in-vitro adhesion study of the dried ITH entrapped microparticles for each formulation was performed using the agar plate method, and particles were found to have good adhesion.

3.6. In-vitro floating study.

We conducted a floating test to determine whether the prepared microparticles were able to float. The lag time of floating microparticles was zero. More than 87% of microparticles remained floating after 12 hours for all formulations. Because nearly all formulations of the generated microparticles remained buoyant following the buoyancy test period, the investigating factors did not affect their floating ability (12 h). Because there was no floating lag period, the microparticles' initial density in 0.1 N HCl was less than 1.004.

3.7. UV- Calibration curve.

The calibration curve of ITH was prepared in 0.1N HCl with the stock solution of 100 mcg/ml in HCl. Aliquots of stock solution were converted into different dilution rages from 10-60 mcg/ml. The lambda max was verified using a 10ppm solution and scanned between 400-200 nm. The absorbance of the above solutions was taken at selected λmax against the blank solution, and a graph of absorbance vs. concentration was plotted, shown in Figure 5.

3.8. In-vitro drug release.

The in-vitro drug release studies were carried out to formulate EC: ES100 microparticles containing ITH prepared with optimized parameters predicted from the prediction profiler in 0.1N HCl (pH 1.2). Dissolution studies showed that 96.98% loaded ITH was released in a controlled manner within 12 hours, Figure 3e and 3f and Figure 6. Initially, the drug release was rapid, up to 30 minutes, and then there was a slow release period. The observed initial high drug release was due to the release of the drug near microparticles' surfaces due to adsorption.

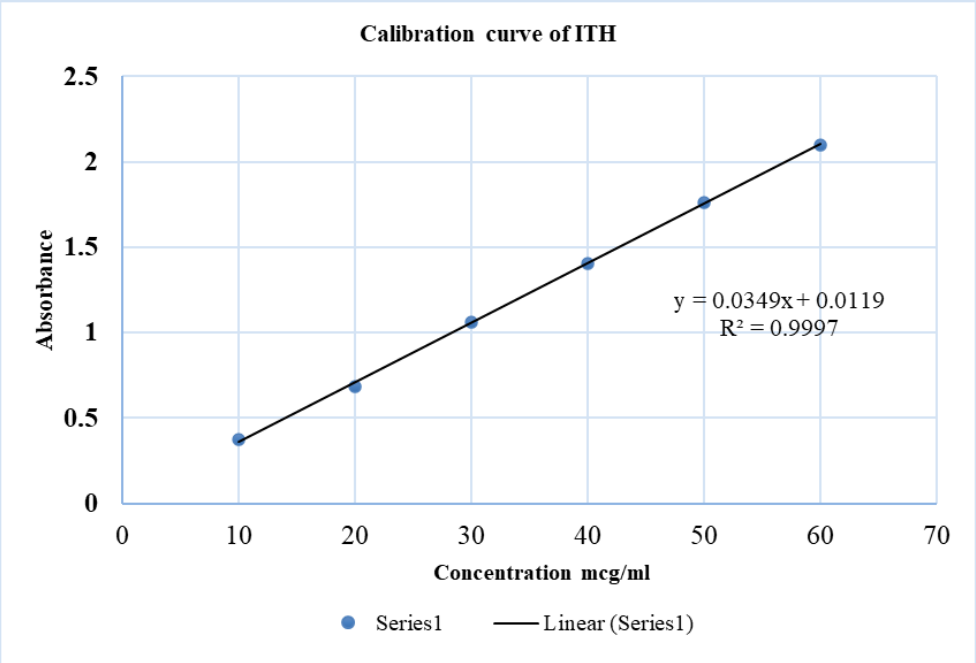

Figure 5. Standard curve of ITH.

The slower release phase was attributed to the portion of the drug that had to be released from the microparticles by diffusion through the media filled pores and channels, leading to slow release. The slow-release continued till the entire amount of drug was released completely.

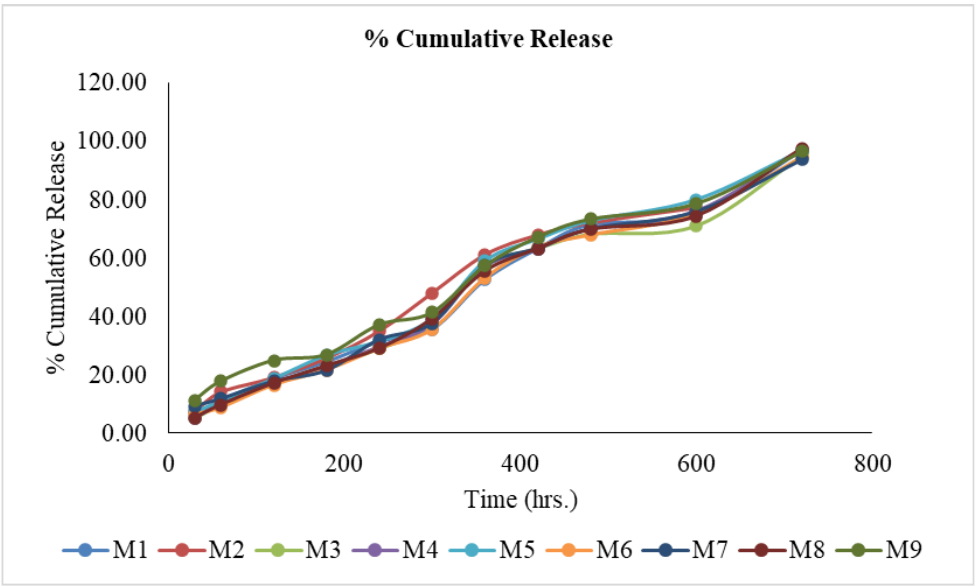

Figure 6. Cumulative drug release from developed formulations.

The in-vitro drug release data from the optimized formulation of EC: ES100 microparticles containing ITH was evaluated kinetically using various mathematical models like zero order, first order, Higuchi, and Korsmeyer–Peppas model. The results of the curve fitting into these above-mentioned mathematical models are given in Table 6. The drug release from these microparticles followed a zero-order model (R^2 = 0.9636) for 12 h. The value of release exponent (n) was determined to be 0.1465, indicating that the transport of the drug across the polymeric matrix takes place by a Fickian diffusion process.

Table 8. Kinetics model with their R2 values.

Kinetic Models	R2	K
Zero order	0.9636	0.1465
First order	0.8265	0.0053
Higuchi plot	0.7810	136.082
Korsmeyer-Peppas	0.3083	0.0972
Hixson Crowell	0.9260	0.0092

3.9. FT-IR spectral analysis.

The drug-loaded formulation's FT-IR spectrum showed characteristic absorption bands at 3453.26 cm^{-1}, 3139.61 cm^{-1}, 2938.02 cm^{-1}, 1635.40 cm^{-1}, 1401.83 cm^{-1}, and 1114.59 cm^{-1}. This indicated that the drug's peak was the same for all batches, and there was no interaction between the excipients in the formulation.

3.10. Stability study of the optimized formulation.

An accelerated stability study was performed on the optimized formulation in accordance with ICH guidelines, and no significant change was found in the drug content on storage, i.e., 94±0.235.

4. Conclusions

The utility of design experts in the optimization of a gastro-retentive mucoadhesive dosage form containing ITH was demonstrated in this work. The solvent evaporation approach was a straightforward, repeatable, and consistent process for the manufacture of these EC and ES floating microparticles containing the ITH system for gastro-retentive administration. The design expert's findings revealed that the polymer to drug ratio and the amount of both polymers used had a significant impact on the dependent variables of drug entrapment efficiency, particle size, and percentage release. Furthermore, the developed formulation has both floating and bioadhesive capabilities, according to in-vitro buoyancy and release experiments. These features allow the microparticles to stick to the gastric mucosal surface and remain in the stomach for an extended period, potentially ensuring the ITH's localized impact on the stomach. Based on the findings, it can be stated that statistical tools such as design experts are very useful in analyzing the connections between multiple independent variables and in developing fast formulations.

Funding

This research received no external funding.

Acknowledgments

The authors are thankful to the GGS College of Pharmacy, Yamunanagar, India, for providing the facilities to carry out the research work.

Conflicts of Interest

The authors declare no conflict of interest.

References

1. Sevinç Özakar, R.; Özakar, E. Current overview of oral thin films. *Turk. J. Pharm. Sci.* **2021**, *18*, 111-121, https://doi.org/10.4274%2Ftjps.galenos.2020.76390.
2. Xiao, Y.; Tang, Z.; Wang, J.; Liu, C.; Kong, N.; Farokhzad, O.C.; Tao, W. Oral insulin delivery platforms: strategies to address the biological barriers. *Angew. Chem. Int. Ed. Engl.* **2020**, *59*, 19787-19795, https://doi.org/10.1002/anie.202008879.
3. Buya, A.B.; Beloqui, A.; Memvanga, P.B.; Préat, V. Self-nano-emulsifying drug-delivery systems: from the development to the current applications and challenges in oral drug delivery. *Pharmaceutics* **2020**, *12*, 1194, https://doi.org/10.3390/pharmaceutics12121194.
4. Ulker Turan, C.; Metin, A.; Guvenilir, Y. Controlled release of tetracycline hydrochloride from poly(ω-pentadecalactone-co-ε-caprolactone)/gelatin nanofibers. *Eur. J. Pharm. Biopharm.* **2021**, *162*, 59-69, https://doi.org/10.1016/j.ejpb.2021.02.009.
5. Flores-Arriaga, J.C.; Chavarría-Bolaños, D.; Pozos-Guillén, A.J.; Escobar-Barrios, V.A.; Cerda-Cristerna, B.I. Synthesis of a PVA drug delivery system for controlled release of a Tramadol-Dexketoprofen combination. *J. Mater Sci. Mater Med.* **2021,** *32*, 56, https://doi.org/10.1007/s10856-021-06529-3.
6. Yu, C.; Lu, P.; Liu, S.; Li, Q.; Xu, E.; Gong, J.; Liu, S.; Yang, C. Efficiency of deoxynivalenol detoxification by microencapsulated sodium metabisulfite assessed via an in vitro bioassay based on intestinal porcine epithelial cells. *ACS Omega* **2021,** *6*, 8382-8393, https://doi.org/10.1021/acsomega.1c00117.
7. Schneider, F.; Hoppe, M.; Koziolek, M.; Weitschies, W. Influence of postprandial intragastric pressures on drug release from gastroretentive dosage forms. *AAPS Pharm. Sci. Tech*. **2018**, *19*, 2843-2850, https://doi.org/10.1208/s12249-018-1022-3.
8. Spósito, L.; Fortunato, G.C.; de Camargo, B.A.F.; Ramos, M.A.D.S.; de Souza, M.P.C.; Meneguin, A.B.; Bauab, T.M.; Chorilli, M. Exploiting drug delivery systems for oral route in the peptic ulcer disease treatment. *J. Drug Target* **2021**, *29*, 029-1047, https://doi.org/10.1080/1061186x.2021.1904249.
9. Balt, J.C.; Klaver, M.N.; Mahmoodi, B.K.; van Dijk, V.F.; Wijffels, M.C.E.F.; Boersma, L.V.A. High-density versus low-density mapping in ablation of atypical atrial flutter. *J. Interv. Card Electrophysiol*. **2021**, *62*, 587-599, https://doi.org/10.1007/s10840-021-00939-7.
10. Das, S.; Kaur, S.; Rai, V.K. Gastro-retentive drug delivery systems: a recent update on clinical pertinence and drug delivery. *Drug Deliv. Transl. Res.* **2021,** *11*, 1849-1877, https://doi.org/10.1007/s13346-020-00875-5.
11. Tripathi, J.; Thapa, P.; Maharjan, R.; Jeong, S.H. Current state and future perspectives on gastroretentive drug delivery systems. *Pharmaceutics* **2019**, *11*,193, https://doi.org/10.3390/pharmaceutics11040193.
12. Srivastava, A.; Verma, A.; Saraf, S.; Jain, A.; Tiwari, A.; Panda, P.K.; Jain, S.K. Mucoadhesive gastroretentive microparticulate system for programmed delivery of famotidine and clarithromycin. *J. Microencapsul.* **2021**, *38*, 151-163, https://doi.org/10.1080/02652048.2020.1851787.
13. Blaesi, A.H.; Saka, N. Expandable fibrous dosage forms for prolonged drug delivery. *Mater. Sci. Eng.: C* **2021**, *120*, 110144, https://doi.org/10.1016/j.msec.2019.110144.
14. Yoshida, V.M.; de Oliveira Junior, J.M.; Gonçalves, M.M.; Vila, M.M.; Chaud, M.V. Development and evaluation of a floating multiparticulate gastroretentive system for modified release of AZT. *AAPS Pharm. Sci. Tech.* **2011**, *12*, 658-664, https://doi.org/10.1208/s12249-011-9627-9.
15. Dhaliwal, S.; Jain, S. Singh, H.P.; Tiwary, A.K. Mucoadhesive microspheres for gastroretentive delivery of acyclovir: *in vitro* and in vivo evaluation. *The AAPS J.* **2008**, *10*, 322-330, https://doi.org/10.1208/s12248-008-9039-2.
16. Rimawi, I.B.; Muqedi, R.H.; Kanaze, F.I. Development of Gabapentin expandable gastroretentive controlled drug delivery system. *Sci. Rep.* **2019**, *9*, 11675, https://doi.org/10.1038/s41598-019-48260-8.
17. Aleksovski, A.; Dreu, R.; Gašperlin, M.; Planinšek, O. Mini-tablets: a contemporary system for oral drug delivery in targeted patient groups. *Expert Opin. Drug Deliv.* **2015**, *12*, 65-84, https://doi.org/10.1517/17425247.2014.951633.
18. Jiang, H.; Tian, R.; Hu, W.; Jia, Y.; Yuan, P.; Wang, J.; Zhang, L. Formulation and evaluation of gastroretentive floating drug delivery system of dipyridamole. *Drug Dev. Ind. Pharm.* **2015**, *41*, 674-80, https://doi.org/10.3109/03639045.2014.893355.
19. Razali, S.; Bose, A.; Chong, P.W.; Benetti, C.; Colombo, P.; Wong, T.W. Design of multi-particulate "Dome matrix" with sustained-release melatonin and delayed-release caffeine for jet lag treatment. *Int. J. Pharm.* **2020**, *587*, 119618, https://doi.org/10.1016/j.ijpharm.2020.119618.

20. Marzouk, M.A.; Osman, D.A.; Abd El-Fattah, A.I. Formulation and *in vitro* evaluation of a thermoreversible mucoadhesive nasal gel of itopride hydrochloride. *Drug Dev. Ind. Pharm.* **2018**, *44*, 1857-1867, https://doi.org/10.1080/03639045.2018.1504059.
21. Kim, Y.S.; Kim, T.H.; Choi, C.S.; Shon, Y.W.; Kim, S.W.; Seo, G.S.; Nah, Y.H.; Choi, M.G.; Choi, S.C. Effect of itopride, a new prokinetic, in patients with mild GERD: a pilot study. *World J. Gastroenterol.* **2005**, *11*, 4210-4214, http://dx.doi.org/10.3748/wjg.v11.i27.4210.
22. Yasin, H.; Al-Taani, B.; Salem, M.S. Preparation and characterization of ethylcellulose microspheres for sustained-release of pregabalin. *Res. Pharm. Sci.* **2020**, *16*, 1-15, https://doi.org/10.4103/1735-5362.305184.
23. Rawat, M.; Saraf, S. Formulation optimization of double emulsification method for preparation of enzyme-loaded Eudragit S100 microspheres. *J. Microencapsul.* **2009**, *26*, 306-314, https://doi.org/10.1080/02652040802319767.
24. Kumari, M.; Gupta, S.K. Response surface methodological (RSM) approach for optimizing the removal of trihalomethanes (THMs) and its precursor's by surfactant modified magnetic nanoadsorbents (sMNP) - An endeavor to diminish probable cancer risk. *Sci. Rep.* **2019**, *9*, 18339, https://doi.org/10.1038/s41598-019-54902-8.
25. Salerno, D.; Jordão, H.; La Marca, F.; Carvalho, M.T. Using factorial experimental design to evaluate the separation of plastics by froth flotation. *Waste Manag.* **2018**, *73*, 62-68, https://doi.org/10.1016/j.wasman.2017.12.001.
26. Paulo, F.; Santos, L. New insights in the *in vitro* release of phenolic antioxidants: The case study of the release behavior of tyrosol from tyrosol-loaded ethylcellulose microparticles during the *in vitro* gastrointestinal digestion. *Colloids Surf. B: Biointerfaces* **2020**, *196*, 111339, https://doi.org/10.1016/j.colsurfb.2020.111339.
27. Peng, B.; Imhof, A. Surface morphology control of cross-linked polymer particles via dispersion polymerization. *Soft Matter* **2015**, *11*, 3589-98, https://doi.org/10.1039/C5SM00606F.
28. Hadizadeh, F.; Shamsara, J. Qualitative Estimation of Drug Entrapment Efficiency in Polymeric Nano - Micelles Using Dissipative Particle Dynamics (DPD). *Pharm. Nanotechnol.* **2017**, *5*, 154-161, https://doi.org/10.2174/2211738505666170522152836.
29. Dankyi, B.O.; Amponsah, S.K.; Allotey-Babington, G.L.; Adams, I.; Goode, N.A.; Nettey, H. Chitosan-coated hydroxypropylmethyl cellulose microparticles of levodopa (and carbidopa): *in vitro* and rat model kinetic characteristics. *Curr. Ther. Res. Clin. Exp.* **2020**, *93*, 100612, https://doi.org/10.1016/j.curtheres.2020.100612.
30. Sadeghi, D.; Solouk, A.; Samadikuchaksaraei, A.; Seifalian, A.M. Preparation of internally-crosslinked alginate microspheres: optimization of process parameters and study of pH-responsive behaviors. *Carbohydr. Polym.* **2021**, *255*, 117336, https://doi.org/10.1016/j.carbpol.2020.117336.
31. Kanojia, N.; Singh, S.; Singh, J.; Sharma, N.; Grewal, A.S.; Rani, L.; Thapa, K.; Arora, S. Recent advancements and applications of inhalable microparticles based drug delivery systems in respiratory disorders. *Biointerface Res. Appl. Chem.* **2021**, *11*, 10099-10118, https://doi.org/10.33263/BRIAC132.150.
32. Naseem, F.; Shah, S.U.; Rashid, S.A.; Farid, A.; Almehmadi, M.; Alghamdi, S. Metronidazole based floating bioadhesive drug delivery system for potential eradication of h. pylori: preparation and *in vitro* characterization. *Polymers* **2022**, *14*, 519, https://doi.org/10.3390/polym14030519.
33. Gajendiran, M.; Divakar, S.; Raaman, N.; Balasubramanian, S. *In vitro* drug release behavior, mechanism and antimicrobial activity of rifampicin loaded low molecular weight PLGA-PEG-PLGA triblock copolymeric nanospheres. *Curr. Drug Deliv.* **2013**, *10*, 722-731, http://dx.doi.org/10.2174/15672018113109990002.
34. Patel, J.; Kevin, G.; Patel, A.; Raval, M.; Sheth, N. Development of the UV spectrophotometric method of Olmesartan medoxomil in bulk drug and pharmaceutical formulation and stress degradation studies. *Pharm. Methods* **2011**, *2*, 36-41, https://doi.org/10.4103/2229-4708.81092.
35. Sharma, D.; Sharma, D. Novel swellable/expandable gastroretentive floating films of gliclazide folded in capsule shell for the effective management of diabetes mellitus: formulation development, optimization and *in vitro* evaluation. *Curr. Drug Ther.* **2021**, *16*, 100-112, http://dx.doi.org/10.2174/1574885515999201201122710.
36. Mhlanga, N.; Ray, S.S. Kinetic models for the release of the anticancer drug doxorubicin from biodegradable polylactide/metal oxide-based hybrids. *Int. J. Biol. Macromol.* **2015**, *72*, 1301-1307, https://doi.org/10.1016/j.ijbiomac.2014.10.038.
37. Jain, A.; Jain, S.K. In vitro release kinetics model fitting of liposomes: an insight. *Chem. Phys. Lipids* **2016**, *201*, 28-40, https://doi.org/10.1016/j.chemphyslip.2016.10.005.

38. Kim, Y.; Park, E.J.; Kim, T.W.; Na, D.H. Recent progress in drug release testing methods of biopolymeric particulate system. *Pharmaceutics* **2021**, *13*, 1313, https://doi.org/10.3390/pharmaceutics13081313.
39. Song, Y.; Cong, Y.; Wang, B.; Zhang, N. Applications of Fourier transform infrared spectroscopy to pharmaceutical preparations. *Expert Opin. Drug. Deliv.* **2020**, *17*, 551-571, https://doi.org/10.1080/17425247.2020.1737671.
40. Nguyen, D.; Secrétan, P.H.; Cotteret, C.; Jacques-Gustave, E.; Greco, C.; Bodemer, C.; Schlatter, J.; Cisternino, S. Stability and formulation of erlotinib in skin creams. *Molecules* **2022**, *27*, 1070, https://doi.org/10.3390/molecules27031070.
41. Puthli, S.; Vavia, P.R. Stability studies of microparticulate system with piroxicam as model drug. *AAPS PharmSciTech.* **2009**, *10*, 872-880, https://doi.org/10.1208/s12249-009-9280-8.